Applications of local crystal structure measures in experiment and simulation

G. J. Ackland* and A. P. Jones
School of Physics, The University of Edinburgh, Mayfield Road, Edinburgh EH9 3JZ, United Kingdom
(Received 30 June 2005; published 9 February 2006)

A general problem in particle-based modeling is one of showing the various configurations which emerge from simulations. A particular problem is to determine the local coordination, distinguishing fcc, hcp, bcc, and other relatively close-packed structures. Here we describe an approach to this problem, which attempts to optimize the *differentiation* between different structure. The method is then applied to differentiate dynamically stabilized phases from mechanically stable ones in bcc crystals, and to identify dislocation defects in random hexagonal close-packed colloidal suspensions, in each case extracting much more information from the raw data than had previously been possible.

DOI: 10.1103/PhysRevB.73.054104 PACS number(s): 61.72.Ff, 81.30.−t, 83.10.Mj, 87.64.Tt

I. INTRODUCTION

In systems as diverse as hard sphere colloids and metallic nanostructures, materials form closely packed structures. To aid in the interpretation of particle-position datasets from molecular dynamics[1] or confocal microscopy,[2,3] it is commonly desirable to determine the local environment, assigning it as fcc, bcc, hcp or some other structure. While this assignment is not unique in relation to crystallography, several schemes have been devised to pick out particular atoms as possible nuclei, defects, or nanocrystals, and color them appropriately. Commonly used coloring methods in atomistic simulation are to color images by cohesive energy,[4] coordination, common neighbor analysis or centrosymmetry,[5–8] while in colloidal materials bond orientation order parameters[9,10] are widely used. In simulations of many millions of atoms, for example in radiation damage studies,[4] it is becoming important to have an efficient method for screening on the fly for those particles whose environments are atypical, so that a manageable amount of data is stored.

Most such methods attempt to match a local structure to an idealized one, and measure how closely they fit. Here we adopt an alternate approach, recognizing that only a finite number of local arrangements will be of interest in a given application, we concentrate on measures which distinguish between them, rather than measures which determine absolute similarity to templates.

Here we report on applications based on a heuristic algorithm to define and analyze the local structure of simulated solids and display the results by color coding particles to reveal regions with bcc, fcc, or hcp crystal structure. The method uses only data routinely calculated in molecular dynamics simulations (i.e., neighbor lists and interatomic vectors) and can readily be incorporated into existing molecular dynamics codes. We present applications of the method to molecular dynamics simulations of martensitic phase transitions and confocal microscopy data of hard sphere colloids.

The challenge is to find an efficient way of defining a local crystal structure from an arrangement of atoms. For correctness this definition must be consistent with the crystallographic definition in terms of periodic repeats, and for usefulness it must assign a local structure to a majority of particles in the system. It must avoid errors arising from the displacement of particles from their symmetry positions, without using an average over millions of atoms to obtain sharp Bragg peaks. It should also define the orientation of the crystal structure.

II. DISTINGUISHING CRYSTAL TYPES: bcc, fcc, and hcp

We take advantage of the preknowledge of the local coordinations which might occur—body centered cubic (bcc), face centered cubic (fcc), and hexagonal close packed (hcp). To determine whether it is realistic to distinguish between these using local separations or angular distributions, we made a large number of samples in each crystal structure and randomly displaced each particle from its perfect lattice site (Fig. 1). This shows that bcc can be distinguished from hcp and fcc by its 14 neighbors, (the two nearest neighbor shells may overlap). fcc and hcp are indistinguishable from near-neighbor analysis; however, the cosines of the angles between the bonds gives a clear distinction.

Previous work used these radial and angular histograms to compare with each ideal crystal type in turn, and then choose the closest fit to assign a crystal structure to a given particle.[5–7,9,10] We attempted this by directly comparing angular distribution to template structure,[1] or fitting the profile with Laguerre polynomials and comparing coefficients to templates. We found these methods relatively unsuccessful because there are many similarities between all three distributions (e.g., fcc has no unique peaks in either radial or angular distribution functions), and so many regions of the histogram contribute only noise to the difference between types. The radial distribution can usually provide the number of near neighbors, but even here any definition avoiding the fcc second neighbors occasionally fails to count a bcc neighbor when the structure is highly distorted, e.g., at high temperature, so it is desirable that the bcc structural determination is robust against missing a neighbor. If neighbors are missed some other methods (e.g., common neighbor analysis[5–7]) will fail. Measures involving "bond order parameters," which are invariant combinations of spherical harmonics,[8,9] are less sensitive to missed neighbors but are relatively slow to calculate.

Since the intention of our work is to provide a practical and efficient method for assigning local crystal structure, we eschew mathematical elegance, and concentrate on heuristics

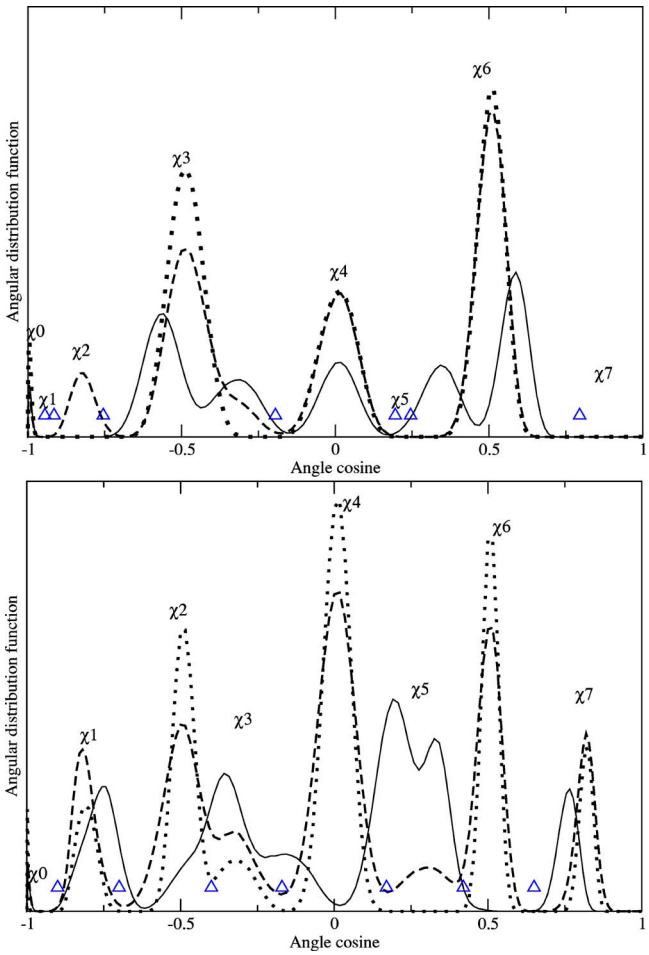

FIG. 1. (Color online) Angular distribution functions; these are frequency distributions of angle cosines among the immediate neighbors of a given particle. They were constructed by randomly moving each particle away from a perfect lattice site within a sphere of radius equal to 0.1 interparticle separations, from its mean "ideal crystal" position. Using the square of the radius saves time calculating roots,[21] while the cosine of the angle is calculated by a simple dot product. The area under each graph is normalized to $N_0(N_0-1)/2$, but since the number of measured nearest neighbors will not always be the same for large displacements the y axis is left dimensionless. (top) bcc shown as the solid line, fcc shown as the dotted line, and hcp shown as the dashed line. Triangles show positions of optimized boundaries between χ_i regions which are used for analysis as described in Table I. (Bottom) a comparison of crystal and amorphous tetrahedral structures, with $r_{ij}<1.8r_0$ to include around 16 neighbors: dots represent the cubic diamond structure, dashes represent the hexagonal diamond, and the solid line is a standard "bc8" model for amorphous silicon (Ref. 22). χ regions in the lower panel are indicative only, and have not been precisely optimized.

which can be rapidly implemented using the information readily available in the radial and angular histograms. Thus, the angular distribution function is described by eight numbers (χ_i), the number of angles in regions of θ_{jik} chosen to reflect angles actually present in the most likely phases (see Fig. 1 and Table I). Distinctive characteristics of combinations of the χ_is were then sought which directly measure differences between the possible structures, and are persistent even under significant deformation.

We examined numerous different configurations to determine the appropriate characteristics—some apparently promising candidates were unsuccessful, e.g., 14 neighbors characterizes bcc, but if two particles stray outside the neighbor range, as may happen at a high temperature, there will be 12 neighbors left: the same as both fcc and hcp, while for fcc and hcp, there may be one or two overlaps between the first and second neighbors. Furthermore, some defect configurations (bcc vacancy, fcc self-interstitial, and atoms in dislocation cores) have different coordinations.

χ_0 (three atoms in a straight line) is a useful measure, since most perfect crystal structures have higher local symmetry than defects. For bcc χ_0 is seven, assuming all 14 neighbors are found; however, if one of the six second neighbors falls outside the "near neighbor" catchment, χ_0 is reduced to six or even five; the most persistent difference between fcc/hcp and bcc turns out to be the ratio of χ_4 (the 90° peak) to everything with lower angles. In fcc/hcp it is 1:2. In bcc it is 1:3 which increases if a second neighbor particle is missed. Even this may fail if the 90° peak broadens beyond the definition of χ_4, so the algorithm incorporates other heuristics (Table II), e.g., if a particle has $\chi_0=7$, $N=14$ it is almost certainly bcc, though the converse is not true.

In order to define defects, some particles should not be assigned a structure, e.g., if there are any very acute angles ($\chi_7>0$) or the number of neighbors is far removed from the expected value. In these cases adjusting the neighbor radius may be appropriate. This occasionally finds a fit, but often discrepancies in the angle remain and the particle structure is unassigned.

Distinguishing fcc from hcp is the most difficult challenge. The obvious difference is the χ_2 peak in hcp; however, if it is wide it may overlap two other peaks, so it cannot always be resolved. A more significant identifier is χ_0. The heuristic examines both $(\chi_0, \chi_0+\chi_1+\chi_2)$, expected for fcc to be (6,6) and for hcp (3,9); we use $(\chi_0+\chi_1+\chi_2)$ rather than just χ_1 because this reduces the effect of overlap. Once these heuristics were decided, we optimized the regions of the histogram assigned to each peak according to their ability to resolve structures generated by random displacements from ideal positions.

Such definitions are necessary, but since there is no precise definition of the "bccness", "fccness" or "hcpness," the real test of this method is the insight gained from applying it to real data.

Close-packed fcc-hcp-bcc are the most difficult structures to resolve, and we have concentrated on these here; however, the method is straighforward to apply to any set of crystal structures. For example, the lower panel of Fig. 1 shows the angular distribution for three tetrahedral structures: cubic diamond, hexagonal diamond, and amorphous. We do not have interesting experimental datasets to analyze for which these are clearly the only options, and so we have not attempted to optimize the χ_i regions. However, the amorphous region can readily be distinguished by the region of χ_5, while the wurtzite and diamond can be separated by considering the ratios of $\chi_1+\chi_3$ to $\chi_2+\chi_4+\chi_6$.

TABLE I. Definition of eight regions of bond angle cosines (Ref. 21) in which the weights χ_i are calculated, and the number of such angles in the perfect crystal of bcc, fcc, and hcp (cf. Fig. 1). $\cos\theta_{jik}$ is the angle between $\mathbf{r}_{ij}$ and $\mathbf{r}_{ik}$ with $r_{ij}, r_{ik} < 1.204 r_0$. The table also lists the combinations δ which were optimized to differentiate structures.

	Minimum $\cos\theta_{jik}$	Maximum $\cos\theta_{jik}$	Ideal bcc	Ideal fcc	Ideal hcp
χ_0	−1.0	−0.945	7	6	3
χ_1	−0.945	−0.915	0	0	0
χ_2	−0.915	−0.755	0	0	6
χ_3	−0.755	−0.705	36	24	21
χ_4	−0.195	0.195	12	12	12
χ_5	0.195	0.245	0	0	0
χ_6	0.245	0.795	36	24	24
χ_7	0.795	1.0	0	0	0
δ_{bcc}		$0.35\chi_4/(\chi_5+\chi_6+\chi_7-\chi_4)$			
δ_{CP}		$0.61\lvert 1-\chi_6/24\rvert$			
δ_{fcc}		$0.61(\lvert\chi_0+\chi_1-6\rvert+\chi_2)/6$			
δ_{hcp}		$(\lvert\chi_0-3\rvert+\lvert\chi_0+\chi_1+\chi_2+\chi_3-9\rvert)/12$			

A. Orientation of crystal structure

The orientation of the local crystal structure can also be calculated. This is most likely to be of interest in the case of hcp, which has a unique c axis, or in any study of grain boundaries or where a specific orientation of crystals arises from a phase transformation.[12] To define hcp orientation we use atoms in the basal planes "above" and "below" the atom, related by the characteristic hcp angle measured by χ_2. Their separation vector does not define the c axis, but the line between the mean position of the three particles above and the three below does. To determine which are above and which are below we arbitrarily choose one pair, and label the first particle above. The other is therefore below, its other

TABLE II. Series of rules implemented to differentiate fcc, hcp, and bcc.

(i)	Evaluate mean squared separation $r_0^2 = \sum_{j=1}^{6} r_{ij}^2/6$ for nearest six particles to i.
(ii)	Find N_0 near neighbors with $r_{ij}^2 < 1.45 r_0^2$ and N_1 with $r_{ij}^2 < 1.55 r_0^2$.
(iii)	Evaluate bond angle cosines (Ref. 14) $\cos\theta_{jik}$ between all $N_0(N_0-1)/2$ neighbor pairs of atom i.
(iv)	From bond angle cosines, determine χ_i (Table I).
(v)	Assign any atom with $N_0 < 11$ or $\chi_0 > 0$ as an unknown.
(vi)	If $\chi_0 = 7$, particle is bcc, if $\chi_0 = 6$, particle is fcc, if $\chi_0 = 3$, particle is hcp.
(vii)	From the angle cosines, define deviations from the expected angular distribution δ (Table I).
(viii)	If no $\delta < 0.1$, then structure is unassigned.
(ix)	If $\delta_{bcc} < \delta_{CP}$ and $10 < N_1 < 13$ assign bcc.
(x)	If $N_0 > 12$ the structure is unassigned, otherwise $\delta_{hcp} < \delta_{fcc}$ implies hcp and $\delta_{fcc} < \delta_{hcp}$ gives fcc.

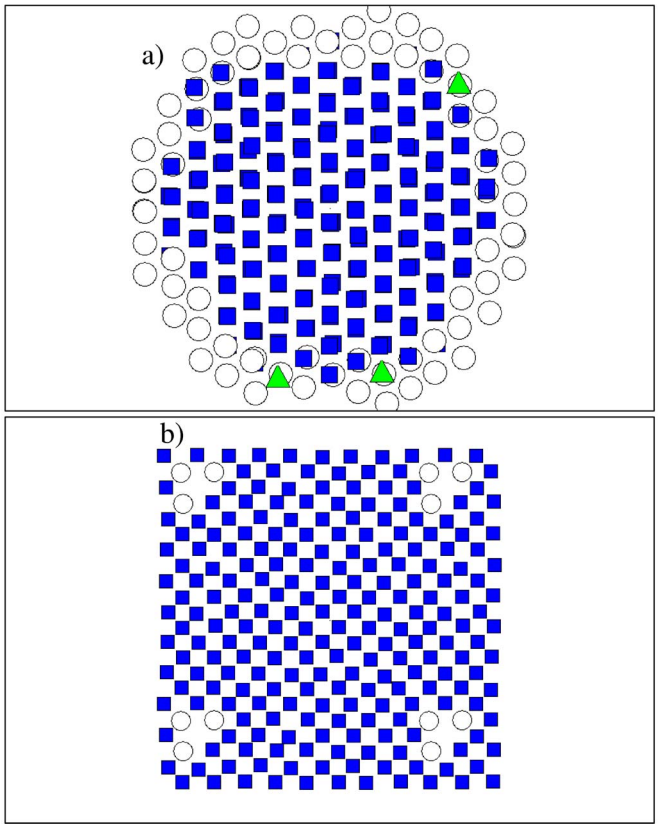

FIG. 2. (Color online) (a) A slice through a snapshot of molecular dynamics of simulated bcc iron (blue squares) with a vacancy in one corner of the cell free boundary conditions. The boundary (surface) atoms are largely unidentified (open circles), although occasionally the 12-fold coordination leads to a misidentification as fcc (green triangles). (b) Rotated view of (a) applying a halo from periodic boundary conditions enables all atoms to be correctly assigned, and the vacancy (and its periodic images) indicated by its unassigned neighbors.

partner forming a χ_2 angle is above, and so forth. This has the advantage that it averages out any small displacements over six particles.

As we shall see, this algorithm is able to correctly identify the instantaneous c axis for all the hcp particles in the high temperature zirconium simulation.

B. Comparison and combination with common neighbor analysis

In this section we compare our present method with one of the methods used in the past. The method chosen is that of common neighbor analysis (CNA).[6,7] Precise timings are arbitrary, as coding efficiency will vary; however, for reasonable implementation neither method is as expensive as a typical molecular dynamics (MD) force analysis. Compared with the present method, the CNA method requires additional a computation as follows.

CNA deals *a priori* with the crystal structure around a bond, not an atom and does not contain explicitly the positions of the particles. Having done the CNA analysis on each bond (for each atom in our method, there are 6/7 bonds for

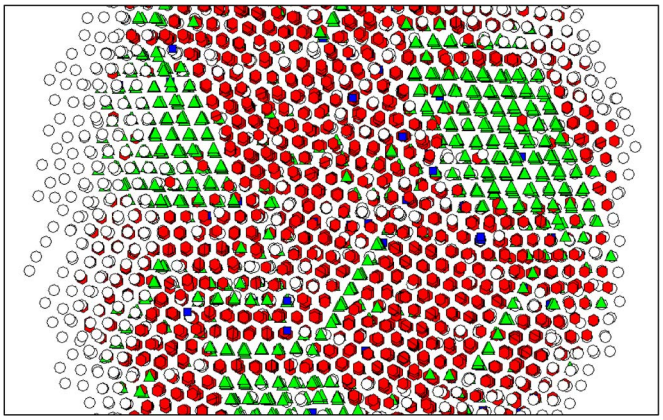

FIG. 3. (Color online) Snapshot from molecular dynamics on simulated bcc zirconium—showing the changing mosaic of fcc (green triangles) and hcp (red hexagons) structures—the data are a cluster cut from the simulation, so surfaces of the data cannot typically be assigned. The zirconium slices show an ever changing pattern of equal amounts of fcc and three different hcp orientations (see also Fig. 5).

CNA to analyze), the local structure at an atom can be found by further analyzing the bonds around that atom. Only then is it possible to identify an atomic level structure. The accuracy of our method and CNA is similar, depending primarily on reliable identification of the neighbors. Whether CNA can find the orientation of hcp regions is debatable; it does not use positional vectors, and none of the CNA bonds point along the hcp c axis hence any orientational information requires considerable analysis "beyond" CNA.

It might be possible to determine the orientation within CNA by adopting the following procedure combining our ideas and those of CNA:

(i) Identify the HCPness of each bond using CNA and project this onto each atom to define an atomic HCPness.

(ii) Re-examine the nearby 421-type[6] bonds to identify what we call the above and below neighbors.

(iii) Distinguish between above and below by a further CNA on each of the above atoms (they are common neighbors of each other, but not of below ones).

(iv) Finally, return to the atomic coordinates as in our method.

III. APPLICATIONS

We have made preliminary images from a number of applications to illustrate how the method can be applied. While statistically significant detailed results from each application will require considerably more data, the images already suggest interesting ideas. Figure 2 shows some slices through configurations analyzed by the method.

Molecular dynamics

1. Point defect in iron

The interstitial defect in iron is unusual in that it is oriented along the (011) direction rather than the more typical (111) adopted by other bcc materials. These defects are gen-

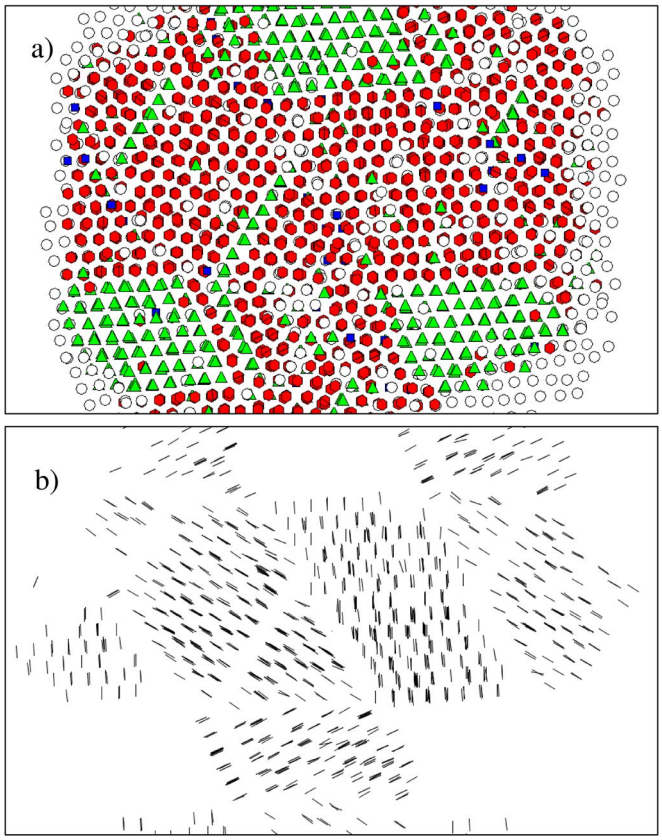

FIG. 4. (Color online) The orientation of hcp "crystallites" in zirconium MD. (a) A snapshot from the MD simulation similar to Fig. 4 (b) Orientation plot: lines show the *c* axis indicating a multiply microtwinned structure, with fcc occurring where we presume that the orientation of the hcp does not permit a low energy interface. Recall that these crystallites are short lived, and the long-range crystal structure in this simulation (determined by simulated x-ray scattering) is bcc. The discrepancy between long- and short-range crystal structure arises from the dynamic instability of the bcc Zr structure.

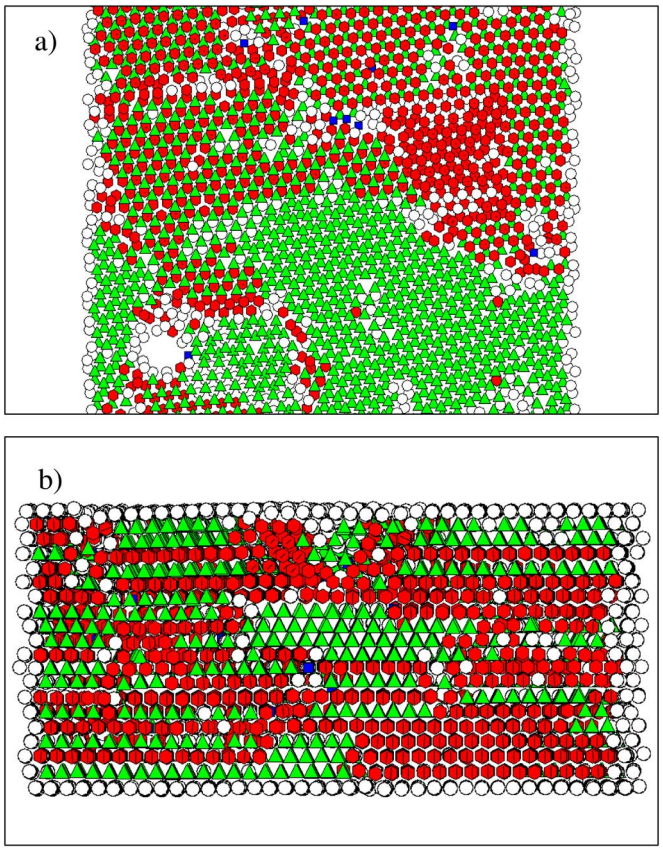

FIG. 5. (Color online) Crystal formed by hard spheres in which the coordinates have been read in using confocal microscopy. Most atoms are assigned fcc (green triangles) or hcp (red hexagons). (a) The view of the crystal down the *c* axis and images of two close-packed layers. Regions of two hcp, two fcc, and one of each can be seen. (b) The view perpendicular to the *c* axis, showing stacking sequence.

erated in large quantities in radiation damage, and for imaging simulations of large scale radiation damage cascades it is desirable to pick out only the defective sites from among millions of perfect lattice sites.

The bcc iron configuration with an interstitial was generated in constant pressure molecular dynamics using the MOLDY code at 200 K with an embedded-atom-type potential derived for use in radiation damage studies for iron[11] which is stable in the bcc structure. The resulting bulk configurations are correctly identified as bcc, despite the thermal vibrations, and the interstitial defect is readily identified from the particles which cannot be assigned to any of the trial structures. It would be possible to generate an angle template for (011) and (111) interstitials using the present method, and reoptimize the algorithm to differentiate them from fcc/hcp/bcc but for illustrative purposes the "unidentified" label is clearly sufficient.

The effect of boundaries is shown in Fig. 2 for a bcc iron configuration with a vacancy in one corner. If the positions from the MD cell are used directly, the boundary atoms are missing neighbors and cannot be identified. If the defect is in this region it will be missed. Adding a halo of additional atoms generated from the periodic boundary condition is sufficient to locate the defect and identify all atoms.

2. Temperature-induced phase transition in zirconium

A more demanding test is a high temperature molecular dynamics run performed using an embedded atom-type zirconium potential.[13]

This potential gives a stable hcp structure, but has a high temperature bcc phase. It has been widely studied[14–17] and there is some controversy about the phase transition temperature which is different depending on how one considers an harmonic terms and the effects of microstructure.[17]

The MD simulation was set up in the bcc phase and allowed to equilibrate at 1100 K. A snapshot cluster cut from the molecular dynamics simulation was analyzed (Fig. 3). Surprisingly, the local structure analysis reveals that most atoms can be characterized as fcc or hcp. This is in contrast to a simulated x-ray diffraction pattern (i.e., a Fourier transform of the entire MD block), which shows that the material has long-range bcc symmetry. Subsequent analysis of the same region showed a similar pattern, but with hcp and fcc regions in different positions, and a movie made from a se-

quence of such snapshots shows a continuous changing of the structure. The ability of our method to resolve the qualitative difference between globally stable bcc iron and dynamically stabilized bcc zirconium shows its value as a compliment to simulated diffraction.

The orientation analysis (Fig. 4) finds boundaries between differently oriented hcp, and indicates that the inter-hcp boundaries are reflection planes (i.e., twins). Moreover, the analysis reveals that the thermodynamically unfavorable fcc structure appears at locations where it can remove the need for nonreflection plane high-energy hcp-hcp boundaries, instead continuing the stacking of close-packed planes (e.g., *ABABABCABC*) to form a very low energy interface.

3. Confocal microscopy images

A final application is to the experimental data taken from the confocal microscopy of *PMMA* (polymethylmethacrylate) hard spheres crystallizing in an index-matched solution in a "random hexagonal close packed" structure.[2,3] Data from this experiment is collected in the form of three-dimensional position coordinates.[18] Previous analysis on this type of configuration has been done by light scattering which determines long range order (equivalent to x-ray diffraction in iron) and by a laborious process of counting stacking faults in appropriately oriented "zigzag" crystals [i.e., viewed along a (-1100) hcp direction].[19] In Fig. 5 our method reveals that regions of local hcp and fcc order appear to be correlated, i.e., although over a large region similar amounts of hcp and fcc layers are seen. An "hcp" layer is more likely to be next to another hcp layer. We also show that partial basal dislocations (indicated by a stripe of one color terminating and becoming the other) are commonplace and can readily be identified, even in the random hexagonal close-packed case. The candidates for screw dislocations are particles which appear in projection to be in ordered positions but are "unassigned" by the analysis, and form columns as one scans downward. Here, the dislocations are often located between an hcp and an fcc layer (i.e., they are partial dislocations). The blue circle in the center of Fig. 3(b) is a bcc-coordinated atom at the center of a curious defect spanning three layers. It is likely that the motion of these defects is significant in the ripening process since their motion converts *ABA* stacking to *ABC*.

Our analysis also identifies an few missing particles and an amorphous "glassy" region in the center of Fig. 3(a) and a near-spherical void (bottom left). In a hard sphere crystal there is no way for a void to be metastable since particles can increase their entropy by moving into it, so it is likely that this "void" is in reality a dust particle which has not been imaged.

In the preceding applications, we did not consider the option of a particle being in an icosahedral cluster (ICO), which may be the stable ordered cluster freezing out of the liquid phase.[20] The angular distribution for ICO is the simplest of all, with six angles at χ_0 and 30 at χ_3 and χ_6. Applying a heuristic which tests for $N_0=12$ and low values of χ_4 relative to χ_3 and χ_6 is sufficient to resolve icosahedral particles in icosahedral clusters.

IV. CONCLUSIONS

We have developed a heuristic approach to defining local crystal structure which fulfills the requirements of being fast to implement within an MD code, giving a low incidence of misassigned or unassigned particles and reproducing the long-range crystal structure for stable perfect crystals. The criteria for defining local crystal structure are necessarily arbitrary, but have been optimized with these features in mind. The approach can be implemented within any application which produces a set of particle positions. In tests it appears to be faster, and to give fewer false positives and negatives than previous methods.

We have tackled the hcp-fcc case which is probably the most difficult, and extensions to other crystal structures are relatively straightforward, as was briefly illustrated for tetrahedral structures. The power of the method in analyzing images is illustrated in three applications, two from simulation and one from experiment. The simulation data involved finding a single point defect in iron, and the more complex study of the local close-packed, strain-compensating nature of dynamically stabilized bcc zirconium. From confocal microscopy data we have shown the existence of voids and dislocation-type defects in random hexagonal close-packed hard sphere crystals.

ACKNOWLEDGMENTS

We thank Matthew Jenkins for supplying the dataset for the colloidal suspension and Iain Bethune for the zirconium md configuration. This work is part of the EPSRC-NANIA collaboration. Code will be available online at homepages.ed.ac.uk/graeme.

*Electronic mail: gjackland@ed.ac.uk

[1] U. Pinsook and G. J. Ackland, Phys. Rev. B **58**, 11252 (1998).
[2] A. van Blaaderen and P. Wiltzius, Science **270**, 1177 (1995).
[3] E. R. Weeks, J. C. Crocker, A. C. Levitt, A. Schofield, and D. A. Weitz, Science **287**, 627 (2000).
[4] D. J. Bacon, Yu. N. Osetsky, R. E. Stoller, and R. E. Voskoboinikov, J. Nucl. Mater. **323**, 152 (2003).
[5] H. Jonsson and H. C. Andersen, Phys. Rev. Lett. **60**, 2295 (1988).
[6] D. Faken and H. Jonsson, Comput. Mater. Sci. **2**, 279 (1994).
[7] J. D. Honeycutt and H. C. Andersson, J. Chem. Phys. **91**, 4950 (1987).
[8] C. L. Kelchner, S. J. Plimpton, and J. C. Hamilton, Phys. Rev. B **58**, 11085 (1998).
[9] J. S. van Duijneveldt and D. J. Frenkel, Chem. Phys. **96**, 4655 (1992).
[10] P. J. Steinhardt, D. R. Nelson, and M. Ronchetti, Phys. Rev. B **28**, 784 (1983).
[11] G. J. Ackland, M. I. Mendelev, D. J. Srolovitz, S. Han, and A. V. Barashev J. Phys.: Condens. Matter **16**, S2629 (2004).
[12] G. J. Ackland, J. Mater. Sci. **40**, 3205 (2005).
[13] G. J. Ackland, S. J. Wooding, and D. J. Bacon, Philos. Mag. A **71**, 553 (1995).

[14] U. Pinsook and G. J. Ackland, Phys. Rev. B **62**, 5427 (2000).
[15] U. Pinsook and G. J. Ackland, Phys. Rev. B **59**, 13642 (1999).
[16] P. Srepusharawoot and U. Pinsook, Phys. Status Solidi B **242**, 1598 (2005).
[17] U. Pinsook, Phys. Rev. B **66**, 024109 (2002).
[18] M. Jenkins (private communication).
[19] M. S. Elliot, B. T. F. Bristol, and W. C. K. Poon, Physica A **235**, 110 (1997).
[20] U. Gasser, E. R. Weeks, A. Schofield, P. N. Pusey, and D. A. Weitz, Science **292**, 258 (2001).
[21] A. P. Sutton, in *Interfacial Structure, Properties, and Design*, edited by M. H. Yoo, W.A.T. Clark, and C. L. Briant, MRS Symposia Proceedings No. 122 (Material Research Society, Pittsburgh, 1988), p. 81.
[22] J. Crain, G. J. Ackland, and S. J. Clark, Rep. Prog. Phys. **58**, 7, 705 (1995).